CRYSTALLISATION FOULING FROM AQUEOUS SOLUTIONS OF CLATHRATE HYDRATES

***A. Karela[1,3], S. M. Clarke[2,3], G. Kawaley[4], A. F. Routh[1,3] and D. I. Wilson[1]**
[1] Department of Chemical Engineering and Biotechnology, University of Cambridge, Cambridge, CB3 0AS, UK
[2] Department of Chemistry, University of Cambridge, Cambridge, CB2 1EW, UK
[3] Centre for Environmental and Industrial Flows, University of Cambridge, Cambridge, CB3 0EZ, UK
[4] Mitsubishi Electric R&D Centre Europe BV, 17 Firth Road, Houstoun Industrial Estate, Livingston, EH54 5DJ, UK

ABSTRACT

Crystallisation fouling from aqueous solutions of 10 - 40 wt% tetrabutylammonium bromide (TBAB) and trimethyloethane (TME) was studied using a two-fingered deposition cell. The clathrates formed semi-solid layers of crystals on the heat transfer surfaces of the cell upon cooling and they reached significant thickness over timescales of one hour. A quantitative model to describe the rate of crystal layer growth was developed based on combined heat transfer and mass transfer control. The model gave a good description of the experimental trends and comparison with the experimental data allowed the estimation of the volume fraction of crystals in the matrix, which approached 40%.

INTRODUCTION

Heating, ventilation and air-conditioning (HVAC) technologies are widely used to provide comfortable indoor environmental conditions by heating or cooling the spaces [1]. Refrigeration is important in HVAC systems and new fluids have been studied for such applications with an aim to increase energy efficiency and reduce environmental concerns [2]. While traditional refrigerants operate by evaporation and condensation of the fluid, a new approach is being considered in order to reduce environmental impact. This is a thermal energy storage technology and involves the use of liquid mixtures containing phase change materials (PCMs); it is based on the solid-liquid phase change, where the PCM absorbs or releases large amounts of energy over a relatively narrow temperature interval [3].

One category of PCMs currently receiving increasing attention are clathrate hydrates. Clathrates are crystalline compounds in which small guest atoms or molecules are physically trapped in host cavities created by a three-dimensional assembly of hydrogen bonded molecules. If the host molecule is water, they are called clathrate hydrates [4]. This study focuses on two potential candidates for use in aqueous solutions as HVAC PCM agents, tetrabutylammonium bromide (TBAB) and trimethylolethane (TME).

TBAB is a quaternary ammonium salt with a bromide counterion. When in aqueous solutions at concentrations up to 50 wt%. the phase change occurs at temperatures between 0-12^{o}C and atmospheric pressure. TBAB forms semi-hydrate clathrate slurries (CHS) with a latent heat of 193-205 kJ kg^{-1} [4]. TBAB solutions have been widely studied as a heat transfer medium [5–8] being potential candidates as a refrigerant because they can reduce pumping power consumption when used instead of chilled water [5].

TME is a polyalcohol and forms one stable clathrate hydrate, TME·3H2O, which melts at 30^{o}C with an associated enthalpy change of 218 kJ mol^{-1} [9]. It is cheaper than other CHS candidates such as TBAB and it is not flammable or corrosive towards metals. There are a few studies on the structure and thermal characteristics of TME [9–11], but it has not been studied extensively as a PCM and there is little knowledge of its solutions' heat transfer characteristics.

Freezing fouling is an important operating challenge for CHS refrigerants. This is a form of crystallization fouling where immobile layers of crystals are formed on the heat transfer surfaces thus reducing the heat transfer effectiveness. Crystal layer formation has been reported for TBAB solutions [7] but has not been studied in detail. The presence of crystals also leads to higher fluid viscosity increasing pressure drops and pumping requirements [7]. Similar studies have been conducted for the processing of semi-solid fat streams in the food industry (e.g. Fernandez-Torres *et al*. [12]) and the formation of wax fouling layers from waxy crude oils on the cold walls of subsea oil pipelines (e.g. Mahir *et al*. [13]).

This paper reports an experimental study of aqueous solutions of TBAB and TME as potential HVAC refrigerant fluids. A novel fouling cell [14] was used to study the effect of solution composition on heat transfer and allowed the growth of fouling

ISBN: 978-0-9984188-2-7; Published online www.heatexchanger-fouling.com

layers to be studied in situ. The rate of fouling layer growth is modelled using a combined heat and mass transfer model. This is based on similar work done by Mahir *et al*. [13] who developed a model that solves the coupled transient energy and mass balances for the precipitation of wax from oil solutions and on the work by Fernandez-Torres *et al*. [12] who derived a combined heat and mass transfer model to describe freezing fouling in food fat distribution pipelines.

MATERIALS AND METHODS

Materials

Ethylene glycol (99.5%), TBAB (50 wt% in H_2O) and TME (solid, ≥ 98% purity) were obtained from Sigma-Aldrich, UK. Aqueous solutions were prepared using distilled water with a resistivity of 18.2 MΩ cm. The solutions were stirred until TBAB or TME were completely dissolved.

Deposition cell

Description of the apparatus. The deposition cell used in this study (shown schematically in Fig. 1a) is an upgraded version of that used by Besevic et al. [14]. The hydrate solution was contained in a 5-litre jacketed vessel and stirred at 70 or 150 rpm by a magnetic stirrer. The cell has two vertical test sections ('fingers') made from either copper or 316L stainless steel (same external dimensions as copper; wall thickness 1 mm). The level of the bulk solution set the area for heat transfer. The dry part of the test sections and the external fittings and pipes were covered with foam pipe insulation. The heating/cooling medium was a 45 wt% aqueous solution of ethylene glycol circulated through the annular gap of the test sections (see Fig. 1b, 1c). T-type thermocouples were used to measure the bulk solution and ambient temperatures as well as that of the coolant entering and leaving each test section. The change in coolant temperature across each test section was used to determine the rate of heat transfer. A cross section of the annular geometry is shown in Fig. 1c.

Experimental series. Two sets of experiments were performed. In the first series of experiments, the jacket was empty and the vessel was filled with distilled water. The test sections were set at 50°C and immersed in the bulk solution. Once the solution reached 50°C, the recirculation was stopped and the bulk temperature was monitored as it cooled in order to quantify the heat loss through the vessel walls. The overall heat transfer coefficient for the test fingers, U_w, was calculated using an overall heat balance (see [15]) at different stirrer speeds and liquid volumes and was found to be around 7 W m^{-2} K^{-1} for all operating conditions.

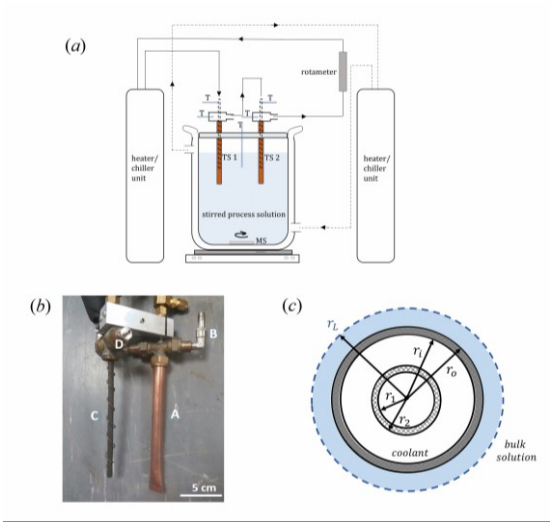

Fig. 1. (*a*) Schematic of the deposition cell, labels: T - thermocouples, TS - test sections, MS – magnetic stirrer; (*b*) photograph, labels: A - test section, B - flow connection, C - flow guide consisting of inlet tube and helical flow guide, D - thermocouple port; (*c*) plan view of annular geometry (r_1 = 2.5 mm, r_2 = 3.25 mm, r_i = 6.85 mm for copper and 6.5 mm for stainless steel, and r_o = 7.5 mm). Radius r_L indicates the interface between the crystal matrix and the bulk solution.

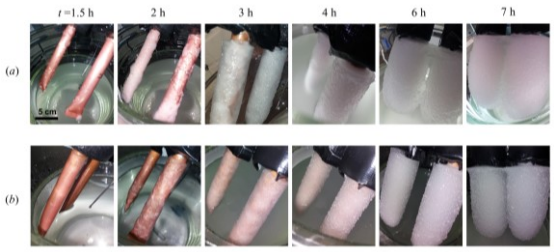

Fig. 2. Time series photographs of crystal matrix formation on the test sections at times indicated for aqueous solutions of (*a*) 40 wt% TBAB and (*b*) 40 wt% TME.

In the second experimental series (freezing fouling), there was no flow in the jacket and the vessel was filled with clathrate solution stirred at 70 rpm. The Reynolds number associated with the magnetic stirrer is given by

$$Re_{stirrer} = \frac{r_{stirrer}^2 \omega_{stirrer} \rho}{\mu} = \frac{\rho}{\mu} 10^{-3} \qquad (1)$$

where $r_{stirrer}$ and $\omega_{stirrer}$ are the radius and rotating speed of the stirrer and ρ and μ the density and viscosity of the bulk solution. $Re_{stirrer}$=400 for 20 wt% TBAB and 452 for 20 wt% TME aqueous solutions at 20°C. The test sections were immersed in the bulk solution and coolant at 30°C was circulated inside the test sections at a flow rate of 3 L min^{-1} until the bulk solution reached this temperature. The set-point on the coolant circulator was then changed to -25°C, removing heat from the clathrate solution. Tests typically ran for seven hours and temperatures were monitored throughout.

ISBN: 978-0-9984188-2-7; Published online www.heatexchanger-fouling.com

Experiments were performed for TBAB and TME aqueous solutions with concentrations of 10-40 wt% and with different combinations of steel and/or copper test sections.

Upon cooling, the solution started to crystallise on the chilled test section surface (Fig. *2*). The lid of the vessel was lifted periodically for a few seconds and the growth of the crystal layer on the test sections was measured using callipers. Crystals were also observed in the bulk solution for TBAB and TME solutions ≥ 20 wt%.

Samples were taken from the crystal matrix and the bulk solution at regular intervals and total organic carbon (TOC) measurements were used to estimate the concentration of the clathrate in the matrix, C_x, and in the bulk, C_{bulk}.

MODELLING OF CRYSTAL LAYER GROWTH

Experimental observations

Fig. 3 is an example of the temperature profiles obtained in an experiment where a crystal layer formed on the chilled finger surface. Four stages are identified. *Step I* is the cooling step, where enthalpy is removed from the bulk solution in the form of sensible heat. *Step II* is the recalescence step where initial crystallization of slightly supercooled solution occurs: latent heat is released, and the temperature increases to a steady value. This step is very fast. *Step III* is the steady growth where a crystal layer builds up on the surface of the test section. The latent heat released is removed by the coolant and there is little change in the temperature of the bulk solution. Eventually, the rate of release of latent heat decreases and sensible heat is also removed from the solution and the decay stage, *Step IV*, is observed.

Similar trends were observed for both TBAB and TME. The equilibrium temperature in *Step III* for a given solution corresponds to the freezing temperature expected from the phase diagrams of the materials [9,16] with no evidence of significant supercooling. The test section material does not affect this temperature. *Step III* was shorter for TME for a given concentration and *Step IV* was sometimes not evident.

Upon cooling, crystallization of the clathrate on the test section begins (*Step III*). A cylinder of particulate gel forms around the test section with radius r_L that grows over time (Fig. *2*).

Fig. 4*a* shows the growth of the crystal layer observed for a 20 wt% solution of TBAB solution with different test section materials; r_L is the radial location of the crystal layer-solution interface and t_0 is the start of the experiment. r_L increases with time at a rate which decreases with time. This behaviour was observed for all TBAB or TME solutions, on copper and SS test sections.

Fig. 4*b* shows concentrations alongside bulk temperature profiles. The concentration of TBAB in the matrix is slightly higher than the initial bulk concentration and increases gradually over time, while that of the bulk solution decreases. This behaviour and the values of the concentration, agree with the trend expected from the phase diagram [9,16].

Heat and mass transfer model

The growth of the crystal matrix layer could be controlled by either heat or mass transfer, or both. In this study, a 1-D combined heat and mass transfer model based on the work by Fernandez-Torres *et al.* [12] was developed to describe the clathrate crystal growth on the heat transfer surfaces. The model describes the experimental trend reasonably well. A summary is presented here: a full account is given in [17].

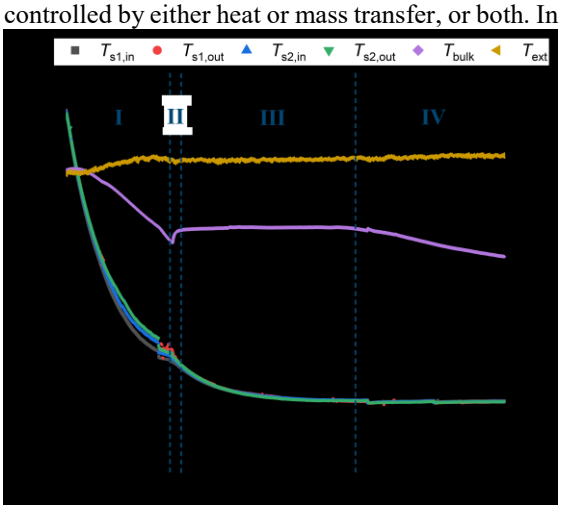

Fig. 3. Evolution of temperatures during cooling of 30 wt% TBAB solution, stainless steel test sections. Vertical dashed lines delineate stages in the cooling process: (I) cooling, (II) recalescence, (III) steady growth and (IV) decay. Horizontal dotted line indicates steady state temperature, T_{ss}. Subscripts *s1* and *s2* refer to the first and second test section, respectively (See Fig. 1); *in* and *out* are the inlet and outlet temperatures, *bulk* refers to the bulk solution and *ext* to the external (ambient) temperature. The initial cooling rate in *Step I* is approximately 0.1 K/min.

The solution is treated as dilute (the mol fractions studied ranged from 0.006-0.05 for TBAB, 0.02-0.13 for TME). The crystal matrix grows at the freezing front (at r_L, Fig. 1*c)* forming an annulus of crystal matrix. Further crystallization within the annulus is not considered. The volume fraction of crystals at the interface is φ and the concentration of the solute in the liquid around the crystals is C_L. The concentration of solute in the bulk solution is C_{bulk}. A difference in these concentrations will result in mass transfer between the bulk solution and the crystal front. If $C_{bulk} > C_L$ and the temperature at r_L is cold enough, crystal growth will occur, forming a

ISBN: 978-0-9984188-2-7; Published online www.heatexchanger-fouling.com

solid phase with molar density ρ_{ms} dispersed within a liquid of concentration C_L. The molar flow rate of solute towards the crystallization front, Q_m, is given by

$$Q_m = 2\pi r_L L k_m (C_{bulk} - C_L) = 2\pi r_L L k_m C_T (x_{bulk} - x_L) \quad (2)$$

where k_m is the convective mass transfer coefficient, L is the wetted length of the finger, C_T is the total molar concentration in the liquid and x_i is the mol fraction of solute at location i. Over timestep dt this transfer results in growth dr_L.

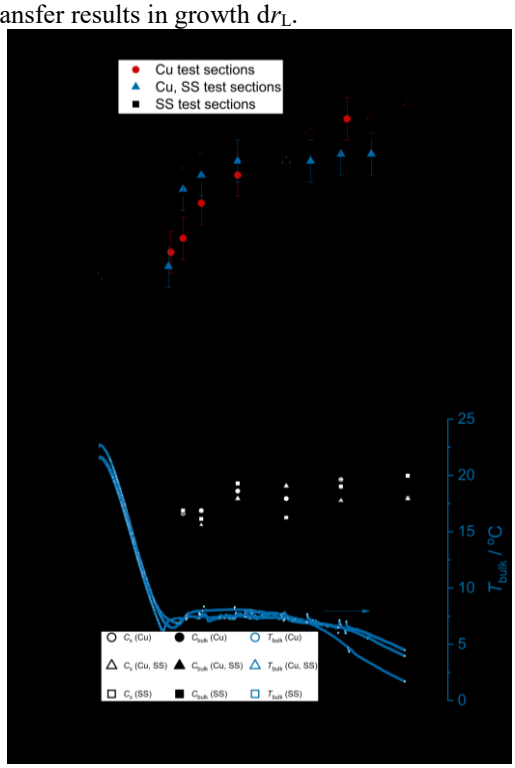

Fig. 4. Example results for cooling of 20 wt% TBAB solution (*a*) Growth of layer; (*b*) Concentration and bulk solution temperature profiles. Solid symbols – concentration in bulk solution; open symbols - crystal matrix. Symbol shape indicates test section material. Horizontal solid line in (*b*) indicates the initial concentration in the bulk. Dotted lines are polynomial fits for the bulk concentration used in the heat and mass transfer model.

A mass balance on the solute gives:

$$2\pi r_L dr_L C_L + 2\pi r_L k_m (C_{bulk} - C_L) dt = 2\pi r_L dr_L [\varphi \rho_{ms} + (1-\varphi) C_L] \Rightarrow \frac{dr_L}{dt} = k_m \frac{(C_{bulk} - C_L)}{\varphi(\rho_{ms} - C_L)} \quad (3)$$

Any change in C_L with radial position is assumed to be small and the system is assumed to be in pseudo-steady state. Using film heat transfer coefficients to describe convective heat fluxes, the temperature at the deposit surface, T_L, can be calculated from the heat balance

$$Q_c = Q_L + Q_m \Delta H \quad (4)$$

where Q_c is the rate of heat transfer from the deposit-bulk interface to the coolant, Q_L the rate of heat transfer from the bulk solution to the interface and ΔH is the enthalpy of fusion of the clathrate. This gives

$$\frac{2\pi L r_o h_i (T_L - T_c)}{\left[1 + \frac{r_o h_i \ln \frac{r_o}{r_i}}{k_{wall}} + \frac{r_o h_i \ln \frac{r_L}{r_o}}{k_x}\right]} = 2\pi L r_L h_L (T_{bulk} - T_L) + 2\pi r_L L k_m C_T (x_{bulk} - x_L) \Delta H \quad (5)$$

where T_{bulk} is the bulk solution temperature, T_c the coolant temperature, h_L the film heat transfer coefficient in the presence of the deposit, h_i the film heat transfer coefficient to the inner side of the outer wall of the annulus, k_{wall} the thermal conductivity of the test section wall and k_x the thermal conductivity of the deposit.

For simplicity, the mixture is assumed to exhibit ideal solution behaviour whereby the freezing temperature, $T_{f,s}$, of solution with solute mole fraction x is given by

$$\ln x = \frac{\Delta H_m}{R}\left(\frac{1}{T_m} - \frac{1}{T_{f,s}}\right) \quad (6)$$

Here T_m is the melting point of pure solute and ΔH_m the enthalpy of fusion. Applying this result to the bulk solution, with mole fraction x_{bulk} and freezing temperature T_b^*, and the deposit interface with mole fraction x_L and freezing temperature T_L, results in the following expression relating x_{bulk} and x_L,

$$x_L = x_{bulk} \exp\left[-\frac{\Delta H_m}{R}\right]\left(\frac{1}{T_L} - \frac{1}{T_b^*}\right) \quad (7)$$

It should be noted that T_b^* is not the temperature of the bulk solution at a given time: it is that in equilibrium with the bulk composition. The solution in contact with the crystal matrix is assumed to be in equilibrium, with T_L set by the coupling of heat and mass transfer. The convective film mass transfer coefficient, k_m, has not been established for the deposition cell and is estimated from the film heat transfer coefficient using the Chilton and Colburn heat and mass transfer analogy.

The film heat transfer coefficient in the presence of the crystal matrix, h_L, can be related to that in the absence of crystals, h_o via

$$Nu = \left(\frac{r_L}{r_o} Re\right)^{\alpha} Pr^{1/3} \Rightarrow h_L r_L = \left(\frac{r_L}{r_o}\right)^{\alpha} h_o r_o \quad (8)$$

where α is a scaling exponent common to heat and mass transfer which will lie in the range $0 \le \alpha \le 1$. Integrating Eq. (3) from $r = r_o$ at $t = 0$ and solving simultaneously with Eq. (5)-(8) gives $r_L(t)$.

k_x was estimated using the Maxwell relationship. Literature data was used for the thermal conductivity and specific heat of H_2O [17], TBAB [8] and TME [9,10]. C_{bulk} was measured using TOC (see Fig. 4*b*). The other parameters used in the model were obtained from literature data and experiments outlined in the following sections (full explanation of the model is given in [15]).

ISBN: 978-0-9984188-2-7; Published online www.heatexchanger-fouling.com

RESULTS AND DISCUSSION

Heat transfer coefficients

Overall heat transfer coefficient, Uf. The overall heat transfer coefficient was estimated from the sensible cooling of the bulk solution, *Step I* in Fig. 3. The solution cools owing to heat transfer to the coolant in the test sections and through the vessel walls, *viz*.

$$mC_P\frac{dT}{dt} = -A_f U_f(T - T_c) - A_w U_w(T - T_{ext}) \qquad (9)$$

Here A_f is the wetted area of the test sections and T_c is the average temperature of the coolant in the sections. The results are presented in Fig. *5* in terms of the Prandtl number, *Pr*. The physical property values are reported in [15]. There is a decrease in U_f with concentration, with the values for TME being larger than those for TBAB solutions at the same concentration, which is a result of the effect of concentration on viscosity. The motion in the bulk solution (which determines the rate of convective heat transfer) is generated by the stirrer, located at the base of the reservoir. The circulation is damped by the liquid viscosity, so the fingers experience lower local velocities in a more viscous fluid.

U_f has slightly higher values for copper test sections compared to stainless steel, which is consistent with the differences in wall thickness and thermal conductivity of the materials. These U_f values correspond to overall Nusselt numbers for the TBAB and TME solutions of ~5-15 and ~12-15, respectively.

Subsequent analysis (detailed in [15]) allowed the calculation of the inner film heat transfer coefficient, h_i, which was found to be ~7600 W m^{-2} K^{-1}.

External film heat transfer coefficient, ho. As the bulk solution cools, heat flows from the solution through the test section to the coolant flowing in the test section annular gap (Fig. 1*c*). Modelling this as steady state heat transfer, with three thermal resistances in series, gives:

$$\frac{1}{U_f r_o} = \frac{1}{h_i r_i} + \frac{\ln r_o/r_i}{k_w} + \frac{1}{h_o r_o} \qquad (10)$$

where k_w is the thermal conductivity of the wall. The radii are identified in Fig. 1*c*. Equation (10) allows the calculation of h_o for TBAB and TME solutions of different concentrations (ranging between 100-700 W m^{-2} K^{-1}). h_o decreases with increasing clathrate concentration for both TBAB and TME, arising from the associated increase in viscous dissipation in the reservoir fluid reducing the local velocity near the fingers. TME gives larger values than TBAB, which is a result of its higher thermal conductivity.

Deposition rate

Fig. 4*a* indicates falling rate fouling behaviour. If the deposition is mass transfer controlled and *Sh* does not change significantly (so $k_m \propto 1/r_L$), then Eq. (3 gives a parabolic relationship of the form ($r_L^2 \propto t$). Data sets plotted in this form are shown in Fig. 6*a* and show an approximately linear trend. The gradients of these trends include a number of parameters determining the rate and are plotted in Fig. 6*b* for all the TBAB and TME solutions concentrations and test sections considered.

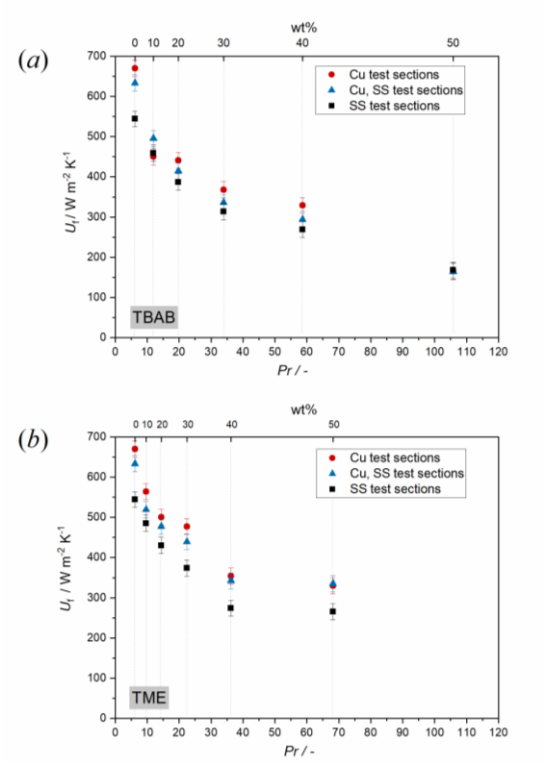

Fig. 5. Effect of (*a*) TBAB and (*b*) TME solution concentration on U_f, composition expressed in terms of *Pr* calculated at 25ºC. Note non-linear scale for mass fractions.

The magnitudes of the gradients are similar for both TBAB and TME. There is noticeable scatter, with no consistent effect of test section material. A weak decreasing trend for TBAB and a weaker increasing trend with concentration for TME are evident.

The results were compared to those predicted by heat transfer control alone or by mass transfer control alone, using the parameters measured or estimated in the above Sections (data not reported). These profiles did not give good agreement with the experimental data, so the coupled model presented earlier was used to describe the crystal growth.

Fig. 7 shows an example of the predictions of the coupled model alongside the experimental data for 20 wt% aqueous TBAB and TME solutions. The main unknowns in this model are the scaling exponent α and the crystal volume fraction φ and different combinations of these two parameters, within expected ranges, were investigated.

In both plots, it is evident that the combined heat and mass transfer model describes the trend in,

ISBN: 978-0-9984188-2-7; Published online www.heatexchanger-fouling.com

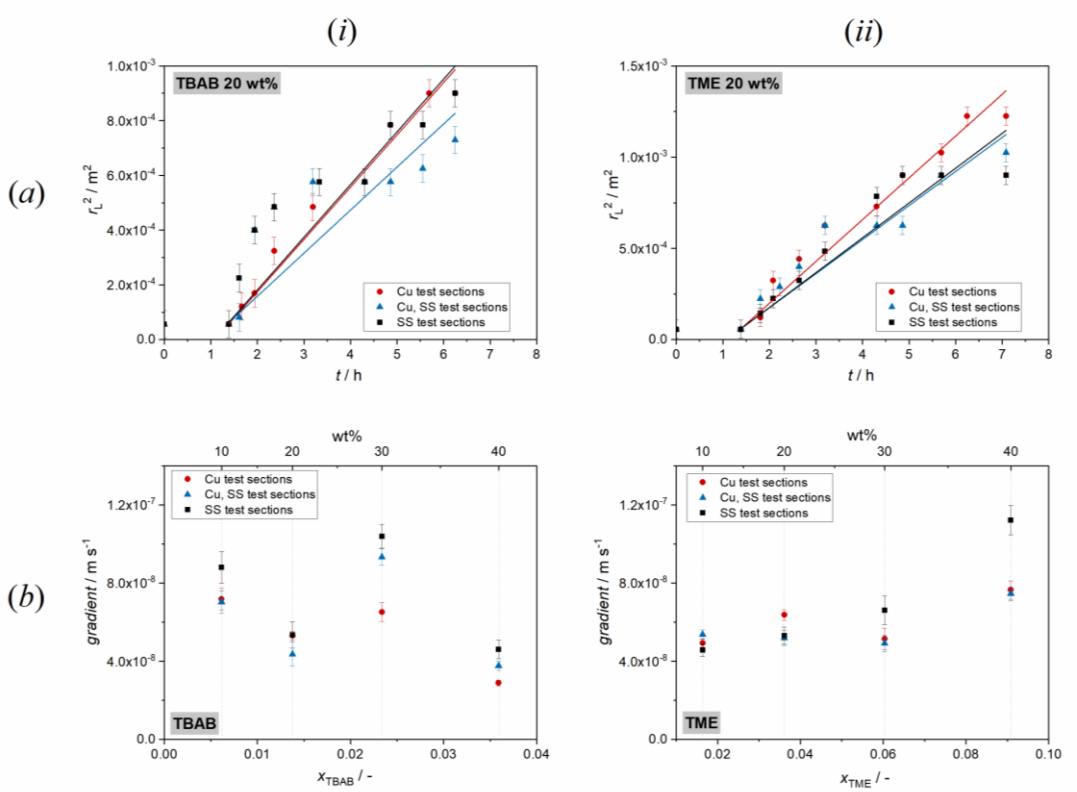

Fig. 6. (*a*) Crystal growth in the form r_L^2 which indicates an approximately linear increase with time, consistent to Eq. (3) if $k_m \propto {}^{1}/_{r_L}$ for (*i*) TBAB 20 wt% and (*ii*) TME 20 wt%. (*b*) Gradients of the linear fit of r_L^2*vs. t* plots for different concentrations of (*i*) TBAB and (*ii*) TME. Symbol shape indicates test section material.

and magnitudes of, the experimental data quite well. Better agreement is obtained when the scaling exponent α is close to zero. Values of α close to 1 would result in a linear increase of r_L over t which is not observed in the experiments (see Fig. 4a). The model also had good agreement to the experimental data, with values of φ=0.2-0.4 for TBAB and φ ~0.2 for TME 20 wt% solutions.

The values of φ obtained for all the concentrations of TBAB and TME solutions studied are presented in Table *1*. For TBAB solutions, φ takes values up to 0.4 for concentrations up to 40 wt%, showing a slight increase with concentration and no evident dependency on the test section material. φ increases to higher values (up to 0.7 for copper and to 0.5 for stainless steel) for 50 wt% TBAB solutions. For TME, φ was around 0.2 for all concentrations when copper sections were used and approached 0.4 for stainless steel sections and lower TME concentrations.

In general, the crystal volume fraction obtained for all solution concentrations, both TBAB and TME, was 40% or less. According to Darbouret *et al*. [18], TBAB hydrate slurries can be transported for φ values up to 40% when crystals are formed in the bulk solution. However, this work indicates that when the shear stress imposed by the flow is not strong enough, the solution will crystallise on the system surfaces at crystal volume fractions below this pumping threshold.

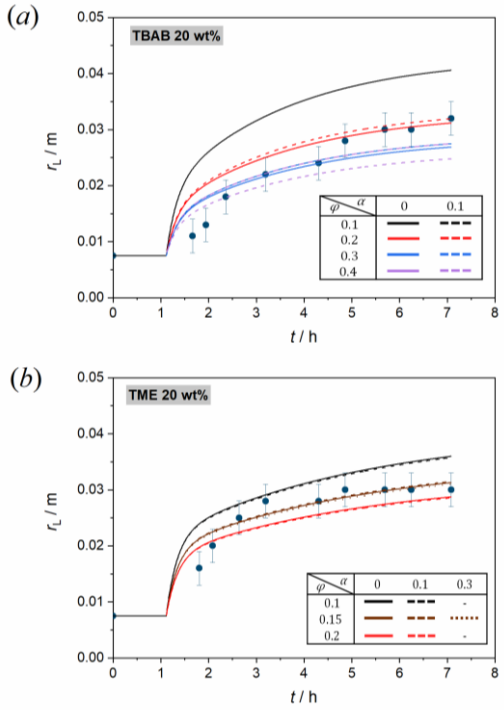

Fig. 7. Combined heat and mass transfer model predictions for 20 wt% (a) TBAB and (b) TME solutions alongside the experimental data obtained with copper test sections. Symbols – data; line colour indicates solids fraction φ, line style indicates scaling exponent α.

ISBN: 978-0-9984188-2-7; Published online www.heatexchanger-fouling.com

Discussion

For clathrate hydrate solutions to be used as refrigerants, different aspects of their behavior must be investigated.

The observation that both TBAB and TME lead to the formation of semi-solid layers of crystals on chiller surfaces over timescales of tens of minutes is significant. In these tests, shear forces by the slow motion of the solution were not sufficient to disrupt the crystal matrix; if such a severe fouling behaviour was observed in a refrigeration system, this would make the system impractical.

The quantitative model describing the rate of layer growth based on combined heat and mass transfer control gave reasonable agreement with the experimental data. There is uncertainty in this work because of the dependence on *Re* and more detailed modelling would require experiments featuring a well-defined flow field.

Measurements of solution and matrix composition over time were included in the coupled model. Since some parameters were estimated, the model could be improved by direct measurement of these quantities (similarly to the work done by Mahir *et al*. [13] on wax solidification) and this would allow its use for the prediction of the expected performance in process-scale devices. The model also allows the estimation of the crystal volume fraction which depends on the concentration of the solution. A more accurate validation of the model would be provided by measuring the crystal volume fraction using techniques like magnetic resonance. However, such measurements are challenging, mostly because of the temperature dependency of the material.

CONCLUSION

The behaviour of TBAB and TME clathrate solutions has been studied at temperatures representative of refrigeration operations. The study was mainly focused on the formation of fouling deposits on chiller surfaces. Cooling caused a deposit layer to form on the chilled heat transfer surfaces over timescales of a few hours for the conditions studied here. A decreasing rate of growth was observed which approached an asymptote as the deposit-solution interface temperature approached the equilibrium temperature. A quantitative model describing the rate of layer growth based on coupled heat and mass transfer control gave a reasonable description of the experimental data, allowing the solids volume fraction in the crystal matrix to be estimated.

ACKNOWLEDGEMENTS

The authors gratefully acknowledge financial support (PhD studentship and project funding) from Mitsubishi Electric R&D Centre Europe B.V as well as from the Onassis Foundation (Scholarship ID: F ZP 019-1/2019-2020).

Table 1. Values of φ obtained from fitting combined heat and mass transfer model to test data.

Concentration (wt%)	φ, TBAB (-)		φ, TME (-)	
Wall material	Cu	SS	Cu	SS
10	0.05 - 0.20	0.05 - 0.20	0.20	0.20 - 0.40
20	0.20 - 0.40	0.10 - 0.30	0.15 - 0.20	0.30 - 0.40
30	0.15 - 0.30	0.05 - 0.20	0.15 - 0.20	0.10 - 0.20
40	0.50 - 0.70	0.30 - 0.50	0.10 - 0.15	0.05 - 0.20

NOMENCLATURE

Roman

α scaling exponent, dimensionless
A_f area of test sections across which heat is transferred, m^2
A_w area of glass wall across which heat is transferred, m^2
c_p specific heat, J/kg K
C_{bulk} molar concentration of the clathrate in the bulk solution, mol/m^3
C_L molar concentration of the clathrate at the solution around the crystal matrix, mol/m^3
C_x molar concentration of the clathrate in the crystal matrix, mol/m^3
h_i inner film heat transfer coefficient, W/m^2 K
h_L heat transfer coefficient in the bulk solution in the presence of the crystal matrix, W/m^2 K
h_o the external heat transfer coefficient in the bulk solution, W/m^2 K
k_m convective mass transfer coefficient, m/s
k_w thermal conductivity of the walls of the section, W/m K
k_x thermal conductivity of crystal matrix, W/m K
L wetted length of test section, m
m mass, kg
Nu Nusselt number, dimensionless
Pr Prandtl number, dimensionless
Q_c rate of heat transfer from deposit interface, W
Q_L rate of heat transfer to deposit interface, W
Q_m molar flow rate, mol/s
r_1 inner radius of inner tube of test section, m

ISBN: 978-0-9984188-2-7; Published online www.heatexchanger-fouling.com

r_2 outer radius of inner tube of test section, m
r_i inner radius of outer wall of test section, m
r_L radius of test section with crystal layer, m
r_o outer radius of outer wall of test section, m
R gas constant, J / K mol
Re Reynolds number, dimensionless
T measured temperature, K
T_{bulk} temperature of bulk solution, K
T_c temperature of coolant inside test sections, K
T_{ext} ambient temperature, K
$T_{f,s}$ freezing temperature of solution, K
$T_{m,i}$ melting temperature of component I, K
T_{ss} steady state temperature, K
T_L temperature at deposit interface, K
U_f overall heat transfer coefficient through test sections, W/m^2 K
U_w heat transfer coefficient from solution to ambient through the glass walls, W/m^2 K
w mass fraction, dimensionless
x mole fraction, dimensionless

Greek

ΔH enthalpy of fusion, J/mol
μ viscosity, Pa s
ρ density of solution, kg/m^3
ρ_{ms} molar density of the clathrate, mol/m^3
φ volume fraction, dimensionless
ω rotation speed, 1/s

REFERENCES

[1] Villafafila-Robles, R. and Salom, J., in *Electrical Energy Efficiency: Technologies and Applications*, pp.335–356, 2012.

[2] Calm, J.M., The next generation of refrigerants - Historical review, considerations, and outlook, *Int. J. Refrig*., 31, pp.1123–1133, 2008.

[3] Du, K., Calautit, J., Wang, Z., Wu, Y. and Liu, H., A review of the applications of phase change materials in cooling, heating and power generation in different temperature ranges, *Appl. Energy.,* 220, pp.242–273, 2018.

[4] Youssef, Z., Delahaye, A., Huang, L., Trinquet, F., Fournaison, L., Pollerberg, C. and Doetsch, C., State of the art on phase change material slurries, *Energy Convers. Manag.*, 2013.

[5] Zhang, P., Ma, Z.W., Bai, Z.Y. and Ye, J., Rheological and energy transport characteristics of a phase change material slurry, 106, pp.63–72, 2016.

[6] Wenji, S., Rui, X., Chong, H., Shihui, H., Kaijun, D. and Ziping, F., Experimental investigation on TBAB clathrate hydrate slurry flows in a horizontal tube: Forced convective heat transfer behaviors, *Int. J. Refrig*., 2009.

[7] Zhou, H., Vasilescu, C. and Infante Ferreira, C., Heat transfer and flow characteristics during the formation of TBAB hydrate slurry in a coil heat exchanger, *Int. J. Refrig*. 64, pp.130–142, 2016.

[8] Ma, Z.W., Zhang, P. and Wang, R.Z., Performance of a cold storage air-conditioning system using tetrabutylammonium bromide clathrate hydrate slurry, pp.1118-1125, 2011.

[9] Yamazaki, M., Sasaki, C., Kakiuchi, H., Osano, Y.T. and Suga, H., Thermal and structural characterization of trimethylolethane trihydrate, *Thermochim. Acta*., 387, pp.39–45, 2002.

[10] Suenaga, K., Matsuo, T. and Suga, H., Heat capacity and phase transition of trimethylolethane, *Thermochim. Acta*., 163, pp.263-270, 1990.

[11] Kakiuchi, H., Yabe, M. and Yamazaki, M., A study of Trimethylolethane hydrate as a phase change material, *J. Chem. Eng. Japan*., 36, pp.788–793, 2003.

[12] Fernandez-Torres, M.J., Fitzgerald, A.M., Paterson, W.R. and Wilson, D.I., A theoretical study of freezing fouling: Limiting behaviour based on a heat and mass transfer analysis, *Chem. Eng. Process*. 40, pp.335–344, 2001.

[13] Mahir, L.H.A., Lee, J., Fogler, H.S. and Larson, R.G. An experimentally validated heat and mass transfer model for wax deposition from flowing oil onto a cold surface, *AIChE J.*, 67, 2021.

[14] Besevic, P., Clarke, S.M., Kawaley, G. and Wilson, D.I., A Novel Fouling Cell To Study Influence of Solution on Crystallisation Fouling, Proc. *Int. Conf. Heat Exchanger Fouling and Cleaning 2017*, Aranjuez (Madrid), Spain, pp.49-57, 2017.

[15] Karela, A., Clarke, S.M., Kawaley, G., Routh A.F. and Wilson D.I., Freezing fouling from aqueous solutions of TBAB and TME clathrate hydrates., *Chem. Eng. Sci.*, under review, 2022.

[16] Aladko, L.S., Dyadin, Y.A., Rodionova, T.V. and Terekhova, I.S, Clathrate hydrates of tetrabutylammonium and tetraisoamylammonium halides, *J. Struct. Chem*., 43, pp.990–994, 2002.

[17] Water - Thermophysical Properties, (n.d.). https://www.engineeringtoolbox.com/water-thermal-properties-d_162.html (accessed February 19, 2022).

[18] Darbouret, M., Cournil, M. and Herri, J., Crystallisation and Rheology of a Hydrate Slurry as Secondary Two-Phase Refrigerant for Air-Conditioning Application, 2005.